A Pressure-Coupled Drucker Function for Plasticity and Fracture Modeling of AA5182

Chong Zhang, Yue Wang, Yanshan Lou, Lei Fu, Saijun Zhang and Jeong Whan Yoon

October 26, 2020

A pressure-coupled Drucker function for plasticity and fracture modelling of AA5182

Chong Zhang[1], Yue Wang[1], Yanshan Lou[1,*], Lei Fu[2], Saijun Zhang[3], and Jeong Whan Yoon[4]

[1] School of Mechanical Engineering, Xi'an Jiao Tong University, 28 Xianning West Road, Xi'an, Shaanxi 710049, China
[2] CHINALCO Materials Application Research Institute Co. Ltd, Beijing 102200, China
[3] School of Mechanical and Automotive Engineering, South China University of Technology, Guangzhou 510640, China
[4] Department of Mechanical Engineering, Korea Advanced Institute of Science and Technology (KAIST), 291 Daehak-ro, Yuseong-gu, Daejeon, 305-701, Republic of Korea

*ys.lou@xjtu.edu.cn

Abstract. In this paper, a pressure-coupled Drucker function is proposed to model the plastic deformation and fracture from shear to plane strain tension of AA5182 sheet. Experiments are conducted for AA5182 in shear, uniaxial tension and plane strain tension, and the force-stroke curves are measured during the tests. The plastic deformation is modeled by the Drucker function. The Drucker function is modified to consider the pressure effect for fracture limit stress prediction of the alloy. The pressure-coupled Drucker function for plasticity and fracture is calibrated by an inverse engineering approach. The calibrated plasticity models are then applied to numerical prediction of plastic deformation of the alloy under various loading conditions. It is observed that the pressure coupled Drucker function accurately describes the plastic deformation under large plastic deformation as well as the onset of ductile fracture under these loading conditions.

1. Introduction

Numerical simulation is now widely used in the design of tools and processes in sheet metal forming. The reliability of simulation calculations largely depends on the accuracy of material models implemented in simulations to describe the plastic behaviour of sheet metals. Accurate description of plastic yielding, strain hardening and fracture are essential to accurately model plasticity during various sheet metal forming processes. There are a class of yield functions which are formulated in forms of the stress invariants. Examples of these yield functions are referred in [1-9]. Cazacu and Barlat extended the Drucker function into an anisotropic form [2]. Lou and Yoon calibrated the Drucker function parameters for BCC and FCC metals [9]. For hardening behaviour evaluation, several hardening models including Swift, Voce, and Swift-Voce model have been widely used [10-12]. In addition, in the last decade, various fracture criteria [13-18] are also proposed for failure prediction of metals. Lou proposed the DF2012 ductile fracture criterion [13] and extended it in 2014 [14] and 2017 [16].

In this study, a yield function is proposed as an equation of the three stress invariants based on the Drucker function to take into account the pressure sensitivity. The pressure-coupled Drucker yield function is combined with the Swift-Voce hardening law to model the plasticity of AA5182 under

various loading conditions of shear, uniaxial tension and plane strain tension. Fracture is also modelled by the pressure-coupled Drucker function for the alloy. The predicted force-stroke curves and the fracture strokes are compared with experimental results to check the accuracy of the pressure-coupled Drucker function for plasticity and fracture.

2. Experiments

Four kinds of specimens with different shapes for different stress states, including dog-bone specimens I, specimens with central hole II, notched specimens III and in-plane shear specimens IV, are designed to study the plasticity and fracture properties of an aluminium alloy of AA5182 with a thickness of 1.26 mm as illustrated in Figure 1. The designed specimens are tested on an electronic universal tensile testing machine of INSTRON 5182 at quasi-static condition with the testing velocities presented in [19]. Figure 1 also shows the initial gauge lengths for stroke measuring by Digital Image Correlation (DIC) of each specimens.

At least 3 experiments were conducted for dog-bone specimens along the rolling direction (RD), diagonal direction (DD), and transverse direction (TD), as shown in Figure 2(a) with good repeatability. The r-values, yield stresses and coefficients of the Swift-Voce law were measured and calibrated for dog-bone specimens along three directions as shown in Table 1. The r-values are calculated by Eq. (1). It is observed that the strength anisotropy of AA5182 in the unidirectional tensile state is not significant. Figure 2(b) shows that both Swift, Voce, and Swift-Voce hardening laws match with the experimental result very well. However, there are big differences between these hardening laws under large deformation after the necking strain.

$$r = \frac{\varepsilon_w^p}{\varepsilon_t^p} = \frac{\varepsilon_w^p}{-\varepsilon_w^p - \varepsilon_l^p} \tag{1}$$

where ε_w^p and ε_l^p is the transverse and longitudinal engineering strain of dog-bone specimen, respectively.

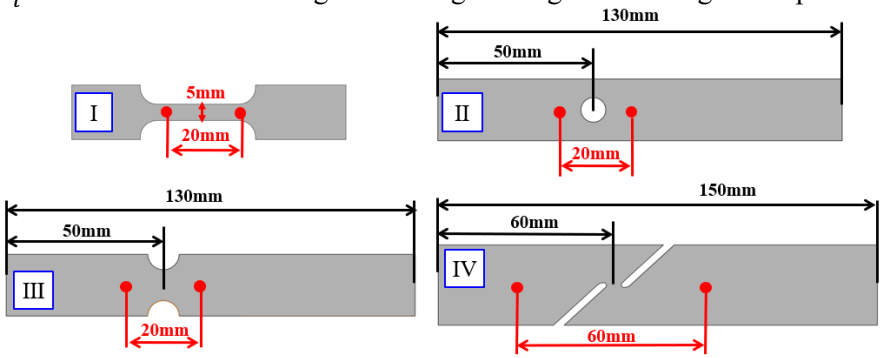

Figure 1. Four specimens for different stress state: (I) dog-bone specimens; (II) specimens with centra l hole; (III) notched specimens; and (IV) in-plane shear specimens

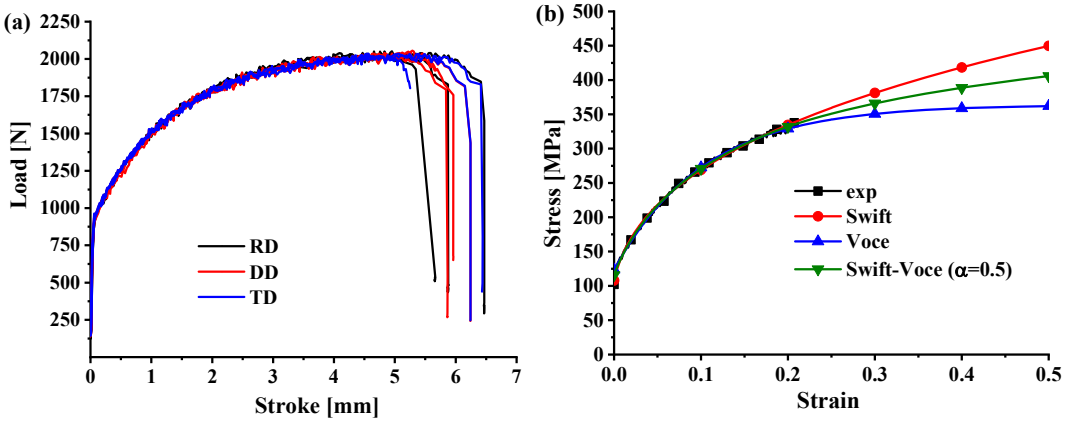

Figure 2. The experiment results of dog-bone specimens: (a) load-stroke curves along three direction; and (b) comparison of stress-strain curve with the Swift, Voce, and combined Swift-Voce laws

Table 1. The R-values, yield stresses and coefficients of the Swift-Voce law calibrated for dogbone specimens along three directions

Loading direction	r-value	Yield stress at 0.2%	Swift			Voce		
			K	e0	n	A	B	C
00	0.527 (#2)	169.8	563	0.0067	0.33	363.9	123.6	9.66
45	0.557 (#1)	166.6	561.5	0.0063	0.33	367.0	122.0	9.45
90	0.5369 (#4)	171	554.7	0.0075	0.324	363.3	129.2	9.44

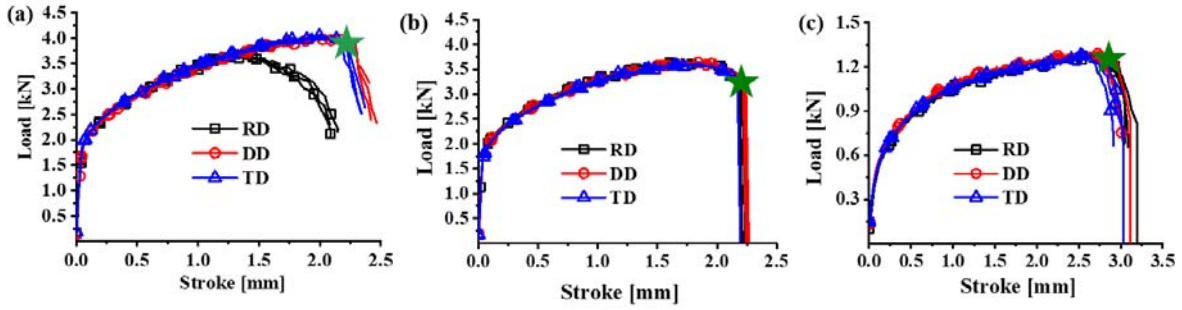

Figure. 3. The load-stroke curves along three direction: (a) specimens with central hole; (b) notched s pecimens; (c) in-plane shear specimens

The load-stroke curves of specimens with central hole, notched specimens, and in-plane shear specimens along three directions are plotted in Figure 3 and the experimental onsets of ductile fracture are indicated by solid pentagrams. For specimens with a central hole, force drops very early along RD compared with those along TD and DD. However, fracture is not observed at load drop along RD and there is no obvious difference observed during the tests for the hole specimens along RD. The mechanism is not clear currently. For other cases, the load-stroke curves show that the anisotropy in strength and fracture is not apparent for this metal. Accordingly, the metal is assumed to be isotropic.

3. Constitutive equations for plasticity and fracture

Lou et al. [20] modified the Drucker yield function to consider the pressure effect as below:

$$\bar{\sigma}(\sigma_{ij}) = a\left(bI_1 + (J_2^3 - cJ_3^2)^{1/6}\right) \tag{2}$$

where a depends on experiments to compute the stress-strain curve, b considers the effect of hydrostatic pressure on yield, and c represents the dependence of yielding on the third invariant. According to Lou and Huh [21], three principal stresses $(\sigma_1, \sigma_2, \sigma_3)$ are transformed by the stress triaxiality η, the Lode parameter L and the von Mises equivalent stress $\bar{\sigma}_{VM}$ as follows:

$$\sigma_1 = \sigma_m + s_1 = \sigma_m + \frac{(3-L)\bar{\sigma}_{VM}}{3\sqrt{L^2+3}} = \left(\eta + \frac{(3-L)}{3\sqrt{L^2+3}}\right)\bar{\sigma}_{VM} \tag{3}$$

$$\sigma_2 = \sigma_m + s_2 = \sigma_m + \frac{2L\bar{\sigma}_{VM}}{3\sqrt{L^2+3}} = \left(\eta + \frac{2L}{3\sqrt{L^2+3}}\right)\bar{\sigma}_{VM} \tag{4}$$

$$\sigma_3 = \sigma_m + s_3 = \sigma_m - \frac{(3+L)\bar{\sigma}_{VM}}{3\sqrt{L^2+3}} = \left(\eta - \frac{(3-L)}{3\sqrt{L^2+3}}\right)\bar{\sigma}_{VM} \tag{5}$$

The third stress invariant of the deviatoric tensor J_3 is derived from equation (2)-(4) as below:

$$J_3 = |s_{ij}| = s_1 s_2 s_3 = -\frac{2L(9-L^2)}{27(L^2+3)^{3/2}}\bar{\sigma}_{VM}{}^3 \tag{6}$$

According to the von Mises yield function $\bar{\sigma}_{VM} = \sqrt{3J_2}$ and the stress triaxiality $\eta = \sigma_m/\bar{\sigma}_{VM} = \frac{I_1}{3\bar{\sigma}_{VM}}$, the J_2 and I_1 can be obtained as follows:

$$J_2 = \frac{\bar{\sigma}_{VM}{}^2}{3} \tag{7}$$

$$I_1 = 3\eta \cdot \bar{\sigma}_{VM} \tag{8}$$

Derived from Eqs. (5)-(7), Eq. (1) can be formulated in terms of η, L and $\bar{\sigma}_{VM}$ in a form of

$$\bar{\sigma}(\sigma_{ij}) = a\left[3b\eta + \left(\frac{1}{27} - c\frac{4L^2(9-L^2)^2}{729(L^2+3)^3}\right)^{1/6}\right]\bar{\sigma}_{VM} \tag{9}$$

If the true stress-true strain curve is measured from uniaxial tensile tests with $\eta = 1/3$ and $L = -1$, the material constant a is given by.

$$a = \frac{1}{b+\frac{1}{3}(27-4c)^{1/6}} \tag{10}$$

In this study, the pressure-coupled Drucker function is used to model the yield surface and fracture limit, while the strain hardening is described by the Swift-Voce hardening law as below:

$$\bar{\sigma} = \frac{\alpha(K(e_0+\bar{\varepsilon}^p)^n)+(1-\alpha)\left(A-(A-B)exp(-C\bar{\varepsilon}^p)\right)}{2} \tag{11}$$

where the values of K, e_0, n, A, B and C are shown in the Table 1.

The pressure-coupled Drucker function is also applied to model the fracture behaviour in this study in a form of as Eq. (12).

$$\bar{\sigma}_f(\sigma_{ij}) = a\left(bI_1 + (J_2^3 - cJ_3^2)^{1/6}\right) \tag{12}$$

where $\bar{\sigma}_f$ is the equivalent stress to fracture.

4. Inverse engineering method for parameter calibration

In order to determine the appropriate parameters in constitutive equations above under large deformation, an inverse engineering method is implemented to calibrate the strain hardening properties under different loading conditions of uniaxial tension, plane strain tension and shear refer to the specimen II, III, IV as shown in Figure 1.

The experimental results of load-stroke curves of three specimens shown in Figure 1 (II)-(IV) are compared with numerical simulations, and the error of each specimens err_m is calculated by Eq. (13). The difference between experiments and prediction is normalized by the average force so that the error between difference strength tests contributes equally to the total error. The total error of three tests, denoted as $Total\_error$, is the sum of three specimens, which is minimized during parameter calibration.

$$err_m = \sqrt{\sum_{i=1}^{n}\left(\frac{F_i^{exp}-F_i^{sim}}{F_{ave}^{exp}}\right)^2} \tag{13}$$

where n is the number of samples, F_i^{sim} and F_i^{exp} is the simulated and experimental values corresponding to the i sample, F_{ave}^{exp} is the average of force values in the experimental load-stroke curves. The averaged force values F_{ave}^{exp} are taken as comparable values to evaluate the relative error between the simulation and experiments on each sample.

b and c in the pressure-coupled Drucker yield function and α value in combined Swift-Voce hardening model are taken as optimization parameters. The optimization goal is to minimize the $Total\_error$, and optimization algorithm utilizes the Downhill Simplex algorithm. The optimized b, c, and α coefficients are shown in the Table 2, as the effect of hydrostatic pressure on yielding and plastic

deformation of this material is extremely small, b value is set to 0, the value of a is obtained from b and c values by Eq. (9).

Similarly, the pressure-coupled Drucker function for the fracture prediction is also optimized by comparing the predicted fracture strokes with experimental results with the inverse engineering method. The parameters are optimized as a=0.2072, b=0.0220 and c=2.6294. The details for the pressure-coupled Drucker fracture function can be referred to Lou and Yoon [9].

5. Results

The optimized coefficients are used in numerical simulation to obtain the load-stroke curves of three specimens and compared with experimental data as plotted in Figure 4. The von Mises yield function is also used in the numerical simulation for the comparison purpose. The comparison of the force-stroke curves shows that the maximum error is mostly less than 2% from the onset of yielding to the ultimate fracture. Therefore, the pressure-coupled Drucker yield function calibrated by inverse engineering approach can accurately predict the plastic behaviour up to large plastic deformation till the onset of ductile fracture. The predicted onset of fracture is also compared with experimental results and the comparison proves that the pressure-coupled Drucker function accurately models the fracture behaviour of the alloy at different loading condition of shear, uniaxial tension and plane strain tension.

Table 2. Coefficients of the pressure-coupled Drucker function and the Swift-Voce hardening law

Pressure-coupled Drucker function			Swift-Voce hardening law						
a	b	c	K	e0	n	A	B	C	α
1.8368	0	2.0045	563	0.0067	0.33	363.9	123.6	9.66	0.0032

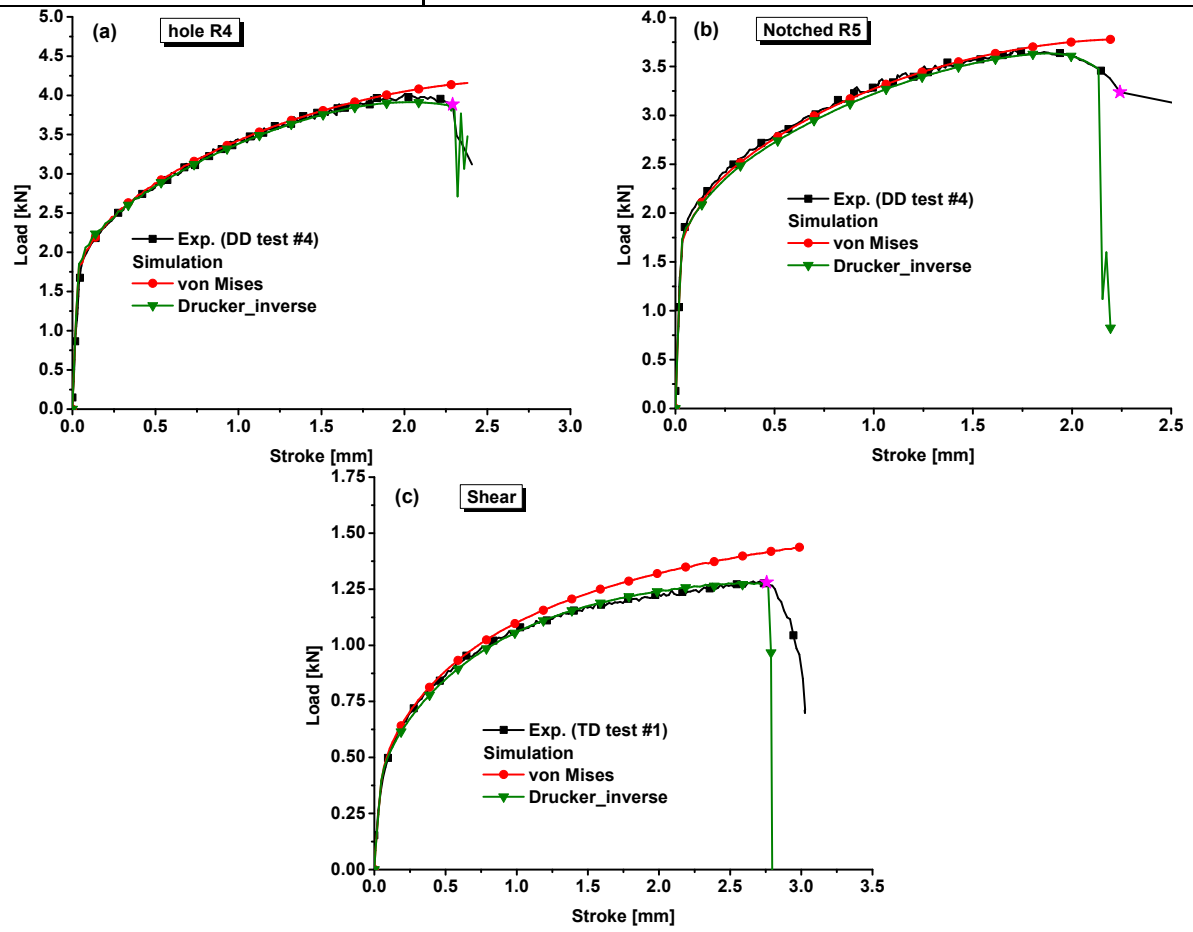

Fig. 4. Load-stroke curve comparison between experiments and prediction: (a) specimens with central hole; (b) notched specimens; (c) in-plane shear specimens

6. Conclusions

This paper modifies the Drucker function to consider the pressure effect of yielding and fracture. The pressure-coupled Drucker function is calibrated using inverse engineering approach for plasticity and fracture of AA5182. The numerical prediction results show that the pressure-coupled Drucker function reasonably predicts the plasticity and fracture stroke for the alloy under various loading conditions including uniaxial tension, plane strain tension and shear. Therefore, the pressure-coupled Drucker function is suggested to plasticity and fracture modelling at different stress states for sheet metal forming processes.

Acknowledgement

The authors acknowledge the financial support by the State Key Laboratory of Mechanical System and Vibration (Grant No. MSV202009), and the State Key Laboratory of High Performance Complex Manufacturing (Grant No. Kfkt2019-02).

References

[1] Drucker, D.C., 1949. Relations of experiments to mathematical theories of plasticity. J. Appl. Mech. 16, 349–357.

[2] Cazacu, O., Barlat, F., 2001. Generalization of Drucker's yield criterion to orthotropy. Math. Mech. Solids 6, 613–630.

[3] Cazacu, O., Barlat, F., 2004. A criterion for description of anisotropy and yield differential effects in pressure-insensitive metals. Int. J. Plast. 20, 2027–2045.

[4] Gao, X.S., Zhang, T.T., Zhou, J., Graham, S.M., Hayden, M., Roe, C., 2011. On stress-state dependent plasticity modeling: significance of the hydrostatic stress, the third invariant of stress deviator and the non-associated flow rule. Int. J. Plast. 27, 217–231.

[5] Yoshida, F., Hamasaki, H., Uemori, T., 2013. A user-friendly 3D yield function to describe anisotropy of steel sheet. Int. J. Plast. 45, 119–139.

[6] Yoon, J.W., Lou, Y., Yoon, J.H., Glazoff, M.V., 2014. Asymmetric yield function based on the stress invariants for pressure sensitive metals. Int. J. Plast. 56, 184–202.

[7] Smith, J., Liu, W.K., Cao, J., 2015. A general anisotropic yield function for pressure-dependent materials. Int. J. Plast. 75, 2–21.

[8] Cazacu, O., Revil-Baudard, B., 2017. New analytic criterion for porous solids with pressure-insensitive matrix. Int. J. Plast. 89, 66–84.

[9] Lou, Y., Yoon, J.W., 2018. Anisotropic yield function based on stress invariants for BCC and FCC metals and its extension to ductile fracture criterion. Int. J. Plast. 101, 125–155.

[10] Kim, J.H., Serpantié, A., Barlat, F., Pierron, F., Lee, M.G., 2013. Characterization of the post-necking strain hardening behavior using the virtual fields method. Int. J. Solids Struct. 50, 3829–3842.

[11] Pham, Q.T., Lee, B.H., Park, K.C., Kim, Y.S., 2018. Influence of the post-necking prediction of hardening law on the theoretical forming limit curve of aluminium sheets. Int. J. Mech. Sci. 140, 521–536.

[12] Li, X., Roth, C.C., Mohr, D., 2019. Machine-learning based temperature- and rate-dependent plasticity model: Application to analysis of fracture experiments on DP steel. Int. J. Plast. 118, 320–344.

[13] Lou, Y. Huh, H., Lim, S., Pack, K., 2012. New ductile fracture criterion for prediction of fracture forming limit diagrams of sheet metals. Int. J. Solids Struct. 49, 3605-3615.

[14] Lou, Y., Yoon, J.W., Huh, H., 2014. Modeling of shear ductile fracture considering a changeable cut-off value for the stress triaxiality. Int. J. Plast. 54, 56–80.

[15] Mohr, D., Marcadet, S.J., 2015. Micromechanically-motivated phenomenological Hosford-Coulomb model for predicting ductile fracture initiation at low stress triaxiality. Int. J. Solids Struct. 67/68, 45-55.

[16] Lou, Y., Chen, L., Clausmeyer, T., Tekkaya, A.E., Yoon, J.W., 2017. Modeling of ductile fracture from shear to balanced biaxial tension for sheet metals. Int. J. Solids Struct. 112, 169-184.

[17] Mu, L., Zang, Y., Li, X.L., Stemler, P.M.A., 2017. A micromechanically-motivated phenomenological model for predicting ductile fracture initiation. Procedia Engineering. 207, 2054-2059.
[18] Hu, Q., Li, X., Han, X., Li, H., Chen, J., 2017. A normalized stress invariant-based yield criterion: modeling and validation. Int J. Plast. 99, 248-273.
[19] Lou, Y., Huh, H., 2013. Prediction of ductile fracture for advanced high strength steel with a new criterion: experiments and simulation. J. Mater. Process. Technol. 213, 1284-1302.
[20] Lou, Y., Zhang, S.J., Yoon, J.W., 2020. Strength modeling of sheet metals from shear to plane strain tension. Int. J. Plast. doi.org/10.1016/j.ijplas.2020.102813.
[21] Lou, Y., Huh, H., 2013. Extension of a shear controlled ductile fracture model considering the stress triaxiality and the Lode parameter. Int. J. Solids Struct. 50, 447-455.